Transcriptional regulation of effector-triggered immunity (ETI) in plants: from tissue to cells

Chhillar, H.

Chapter 2

Modular mechanisms of immune priming and growth inhibition mediated by plant effector-triggered immunity

Himanshu Chhillar[1], Hoang Hung Nguyen[1#], Pei-Min Yeh[1#], Jonathan DG Jones[2], Pingtao Ding[1]

[1] Institute of Biology Leiden, Leiden University, Sylviusweg 72, Leiden 2333 BE, The Netherlands
[2] The Sainsbury Laboratory, University of East Anglia, Norwich Research Park, Norwich NR4 7UH, UK
[#] These authors contributed equally

This chapter is published in: Cell Reports (2025) Mar 25;44(3):115394. doi: 10.1016/j.celrep.2025.115394

Abstract

Excessive activation of effector-triggered immunity (ETI) in plants inhibits plant growth and activates cell death. ETI mediated by intracellular Toll/Interleukin-1 receptor/Resistance protein (TIR) nucleotide-binding leucine-rich-repeat receptors (NLRs) involves two partially redundant signaling nodes in *Arabidopsis*, EDS1-PAD4-ADR1 and EDS1-SAG101-NRG1. Genetic and transcriptomic analyses show that EDS1-PAD4-ADR1 primarily enhances the immune component abundance and is critical for limiting pathogen growth, whereas EDS1-SAG101-NRG1 mainly activates the hypersensitive cell death response (HR) but is dispensable for immune priming. This study enhances our understanding of the distinct contributions of these two signalling modules to ETI and suggests molecular principles and potential strategies for improving disease resistance in crops without compromising yield.

Introduction

Inducible plant defense usually involves the concerted action of responses initiated by cell-surface and intracellular immune receptors. Cell-surface pattern recognition receptors (PRRs) initiate pattern-triggered immunity (PTI) upon detection of relatively conserved apoplastic pathogen molecules such as chitin or flagellin. Effector-triggered immunity (ETI) is activated by intracellular nucleotide-binding, leucine-rich repeat receptors (NLRs) upon recognising specific pathogen effector proteins[1,2]. ETI and PTI together confer a highly effective plant defense against pathogen attack[3–5]. Recent research has significantly expanded our understanding of the signalling pathways downstream of Toll/Interleukin-1 receptor/Resistance protein (TIR)-type NLR (TNL)-triggered ETI, with key roles played by lipase-like proteins ENHANCED DISEASE SUSCEPTIBILITY 1 (EDS1), PHYTOALEXIN DEFICIENT 4 (PAD4), and SENESCENCE-ASSOCIATED GENE 101 (SAG101), and helper NLRs

ADR1 (ACTIVATED DISEASE RESISTANCE 1) family and NRG1 (N REQUIREMENT GENE 1) family proteins, which share RESISTANCE TO POWDERY MILDEW 8 [i](RPW8)-like coiled-coil N-terminal signalling domains[2,6].

EDS1, PAD4, and SAG101 have emerged as central TNL signalling regulators in *Arabidopsis thaliana* (Arabidopsis) and many other plant species[7]. These proteins form distinct heterodimeric complexes regulating cell death and disease resistance[8]. EDS1-PAD4 complexes have been shown to play a crucial role in local and systemic acquired resistance (SAR)[9]. Meanwhile, EDS1-SAG101 complexes are hypothesised to be more critical for local immune responses, such as constraining the spread of plant viruses[10]. PAD4 and SAG101 also influence salicylic acid (SA) accumulation, connecting hormonal signalling pathways with the regulation of cell death and disease resistance[11].

The ADR1 family proteins (ADR1s) in Arabidopsis include ADR1, ADR1-LIKE 1 (ADR-L1), and ADR1-L2, which are also known as helper NLR proteins (hNLRs). They are pivotal in controlling ETI[12]. These proteins act as signal amplifiers, promoting the activation of downstream immune responses upon effector recognition[2,13]. The NRG1 hNLR family proteins (NRG1s), including NRG1A (or NRG1.1) and NRG1B (or NRG1.2), are required by TIR-NLRs to drive hypersensitive response (HR) cell death and contributing to enhanced disease resistance against oomycete pathogens[14]. More recently, it has been shown that *pad4* mutant mimics *adr1s,* while *sag101* mutant mimics *nrg1s* in classical immune responses[15–17]. These genetic results align with the model proposed by several groups that EDS1-PAD4 functions together with ADR1s and contributes more to restricting bacterial growth in TNL-mediated ETI, while EDS1-SAG101 functions with NRG1 and contributes more towards TNL-mediated cell death induced by ETI[15–20]. These results indicate two distinct

immune regulatory nodes associated with EDS1, leading to different downstream signalling.

The growth-defense trade-off, where plants slow growth in response to pests, is a key principle in plant economics affecting both ecosystems and crop breeding[21]. Many constitutive ETI mutants with auto-active NLR have shown severe growth penalties[22], which might act via various hormonal signalling while enabling plants to thwart pathogen attacks[23]. Recently, it has been shown that constitutive induction of ETI in the absence of PTI can also effectively lead to significant growth arrest[24]. Additionally, prior exposure of plants to pathogens or pathogen-derived ligands primes the plants to induce a much more robust immune response to subsequent encounters[25]. For instance, multiple PAMPs have already been shown to prime Arabidopsis plants against virulent *Pseudomonas syringae* pv. *tomato* (*Pst*) DC3000 bacterium[26]. ETI-induced priming has recently shown a similar effect[24]. However, the contribution of crucial immune regulators in governing the phenomenon of ETI-mediated growth-defense trade-off and immune priming remains inadequately understood.

In this study, we unravel the modular signalling pathways downstream of TNL-induced ETI mediated by EDS1-PAD4-ADR1s and EDS1-SAG101-NRG1s, with particular emphasis on their roles in cell death, immune priming, and ETI-induced growth arrest. We have also explored differential transcriptional outcomes between EDS1-PAD4 and EDS1-SAG101 nodes. This work advances our understanding of plant immunity and sheds light on potential strategies for improving disease resistance in crops without impinging on growth and yield.

Results

Differential roles of EDS1-PAD4-ADR1s and EDS1-SAG101-NRG1s in ETI-induced growth arrest

All previous immune phenotypes reported for lipase-like/hNLRs mutants were observed during ETI activation in the presence of PTI. Therefore, it was unknown to what extent prior results are ETI-specific. Here, we used a β-estradiol (E2)-inducible AvrRps4-expressing ('SETI') line, to activate TNL-mediated ETI in the absence of PTI via the two paired TIR-NLRs RPS4 and RRS1, and RPS4B and RRS1B[24]. When growing SETI plants on an E2-containing medium, we observed growth arrest, including a reduction in size and fresh weight (**Figure 1A-C**). This growth arrest was suppressed entirely in the *eds1-2* mutant (SETI_*eds1*) and the *pad4 sag101* double mutant (SETI_*ps*), indicating a critical role for EDS1, PAD4, and SAG101 in modulating ETI-induced growth inhibition mediated by TNLs.

However, the *sag101* single mutant (SETI_*sag101*) exhibited a growth inhibition pattern like SETI_wt (**Figure 1A**), implying that SAG101 does not contribute to ETI-induced growth arrest. Interestingly, the *pad4* single mutant (SETI_*pad4*) appeared to partially suppress the ETI-induced growth arrest in the absence of PTI despite having similar induction in AvrRps4 expression (**Figure S1D**), suggesting PAD4 may play a significant role in mediating ETI-dependent growth arrest independent of SAG101 (**Figure 1A**). Curiously, a severe inhibition in lateral root formation was observed in SETI_wt and SETI_*sag101,* which was partially relieved in SETI_*pad4* plants and completely relieved in SETI_*eds1* and SETI_*ps* suggesting a role for *PAD4* in controlling root growth and development (**Figure 1B**).

In parallel, we observed that the *nrg1a nrg1b* double mutant (SETI_*nrg1s*) mirrored the SETI_*sag101* phenotype (**Figure S1A-C**), implying that the

NRG1 family proteins may not contribute to growth arrest in response to ETI. Finally, the *adr1 adr1-l1 adr1-l2* triple mutant (SETI_*adr1s*) resembled the SETI_*pad4* phenotype, suggesting a functional correlation between PAD4 and ADR1 proteins in the regulation of ETI-mediated growth arrest.

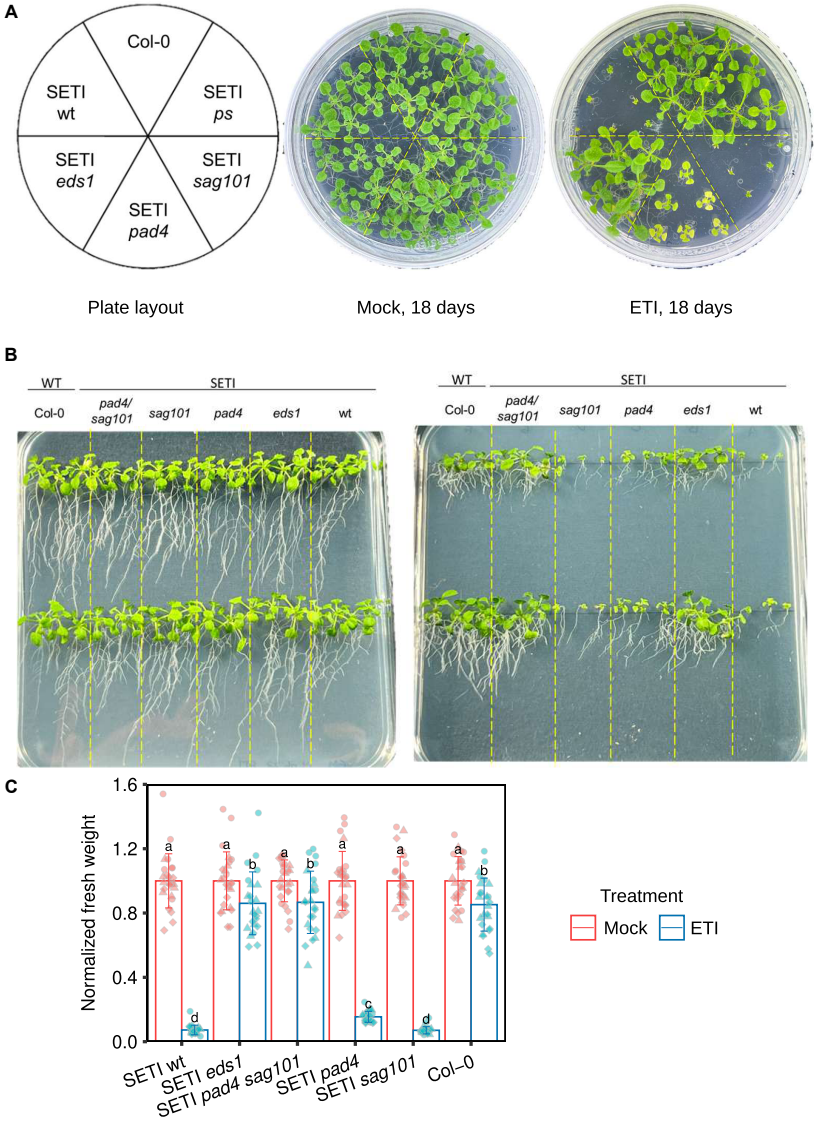

Figure 1. Estradiol induced growth arrest phenotype in lipase-like protein mutants. A. Indicated mutants of lipase-like proteins (SETI_wt, SETI_*sag101*, SETI_*pad4*, SETI_*pad4 sag101*, SETI_*eds1)* were sown on round GM plates with or without E2 (50 µM), and their growth arrest phenotype was recorded 18 days after planting on E2 plates. (Note: We have used the full name of all the mutants

in all the figures for better visualisation). B. Indicated mutants of lipase-like proteins were sown on square GM plates with or without E2 (50 µM), and the plates were grown vertically. Growth arrest and lateral root formation phenotypes were recorded 18 days after sowing on E2 plates. C. Indicated mutant lines were sown vertically on square GM plates with or without E2 (50 µM) and the fresh weight was recorded 18 days after sowing on E2 plates. Fresh weight was normalized to the average fresh weight of the mock controls for the respective lines. The error bars show standard deviation. Letters are highlighting statistical differences (LSD-test, $p \leq 0.05$).

Distinct contributions to ETI-mediated cell death by PAD4-ADR1s and SAG101-NRG1s

SETI_wt shows no macro cell death induced by ETI in the absence of PTI[24]. This hypersensitive response (HR) can be measured by recording ion leakage upon E2 induction, which is easily distinguishable at 4 hours post infiltration (hpi) from the mock treatment and saturates at 22 hpi (**Figure 2A, S2B, S3D**). SETI_*eds1* and SETI_*ps* plants do not show any significant increase in ionic conductivity upon E2 treatment, highlighting the interplay of EDS1, PAD4, and SAG101 in mediating the ETI-mediated cell death.

Interestingly, the increase in ion conductivity in SETI_*pad4* upon E2 induction is similar to SETI_wt, suggesting that PAD4 alone is not sufficient to activate ETI-induced cell death (**Figure 2A**). However, the increase in ion conductivity upon E2 treatment is significantly compromised in SETI_*sag101* plants, showing an independent role of SAG101 from PAD4 in mediating ETI-induced cell death in the absence of PTI (**Figure 2A**). Furthermore, only SETI_*ps* mutant can fully compromise the ETI- induced ion leakage like SETI_*eds1* (**Figure 2A**). This suggests a synergistic contribution of PAD4 and SAG101 to cell death as we only see complete abolishment in ion leakage when both PAD4 and SAG101 are lost. We have also observed similar trends in the hNLR mutants in the

SETI background (SETI_*nrg1s* and SETI_*adr1s*) (**Figure S3A, S3D**). The SETI_*adr1s* mimics SETI_*pad4* while SETI_*nrg1s* mimics SETI_*sag101,* showing that the SAG101-NRG1 node might contribute more to ETI-induced cell death while the PAD4-ADR1 node merely acts as a synergistic module in the presence of the parallel SAG101-NRG1 node.

HR has been shown to have a close association with chlorophyll catabolism[27,28]. Therefore, we sought to test the chlorophyll content as an additional indicator of cell death. A reduction in total chlorophyll content was observed for SETI_wt and SETI_*pad4* upon E2 treatment (**Figure 2B, S2A**), which was intensified significantly upon the 'PTI+ETI' (PTI plus ETI) treatment (50 µM of E2 and *Pst* DC3000 *hrcC*$^-$) which is in line with the previous report[4]. However, in SETI_*sag101*, a significant reduction of the total chlorophyll content is observed after 'PTI+ETI' treatment but not after PTI nor ETI alone (**Figure 2B**). This reduction is not as significant as in SETI_*pad4* and SETI_wt (**Figure 2B**). As expected, there is no reduction in chlorophyll content in SETI_*ps* lines. SETI_*adr1s* also showed a significant reduction in chlorophyll content upon ETI and 'PTI+ETI' treatments (**Figure S3B, S3C**), and this reduction is compromised in SETI_*nrg1s*, which is also in agreement with the ion leakage results that the SAG101-NRG1 node contributes more to ETI-induced cell death.

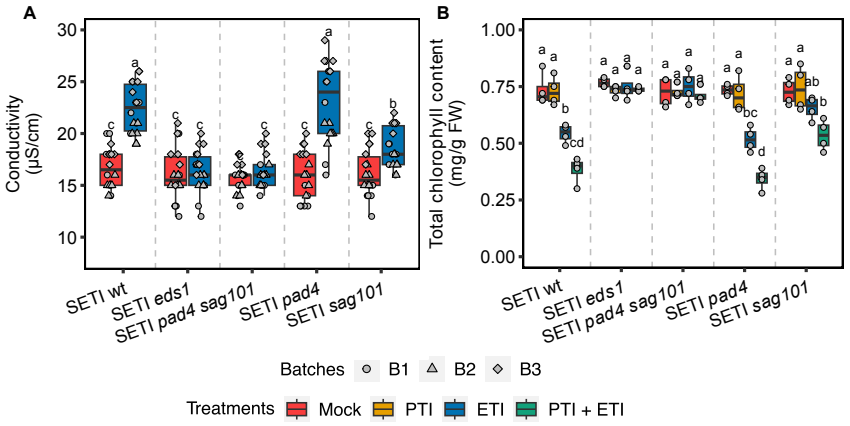

Figure 2. Differential regulation of ETI-induced cell death mediated by lipase-like protein. A. Indicated mutants of lipase-like proteins (SETI_wt, SETI_*sag101*, SETI_*pad4*, SETI_*pad4 sag101*, SETI_*eds1*) were infiltrated with E2 or mock and ion leakage was determined at 24 h time point. Letters showing statistical differences (Tukey-HSD-Test, $p \leq 0.05$). B. Total chlorophyll content was estimated on indicated mutants of lipase-like proteins 3 dpi after E2 infiltration as ETI treatment, *Pst* DC3000 *hrcC*$^-$ as PTI treatment, (E2 + *Pst* DC3000 *hrcC*$^-$) as PTI+ETI treatment and DMSO dissolved in 10 mM $MgCl_2$ as mock. Letters represent statistical differences (Tukey-HSD-Test, $p \leq 0.05$).

ETI-mediated immune priming requires both PAD4-ADR1s and SAG101-NRG1s nodes

Pre-treatment of SETI_wt plants with E2 shows increased disease resistance against subsequent bacterial infection, indicating ETI alone can prime plant immunity[24]. Consistent with this previous report, we also observed a significant reduction in bacterial growth compared to mock control when SETI_wt plants were pre-infiltrated with E2 one day before being inoculated with the virulent bacterial strain, *Pst* DC3000 carrying an empty vector (**Figure 3**). In contrast, E2-pretreated SETI_*eds1* and SETI_*ps* plants show complete loss of priming.

In parallel, we then performed an E2- or ETI-induced disease priming assay with SETI_*pad4* and SETI_*sag101* mutant plants. We found that the E2-pretreated SETI_*sag101* plants show no significant difference from SETI_wt plants in disease resistance priming (**Figure 3**). Similarly, such a priming effect is retained in SETI_*pad4*, though overall bacterial growth in E2-pretreated SETI_*pad4* plants is more than those in SETI_wt and SETI_*sag101* plants (**Figure 3**). It is noteworthy that the *pad4* but not *sag101* mutant was shown to be partially compromised in PTI-primed disease resistance with the elicitor of a 22-amino-acid epitope from bacterial flagellin and fully compromised in nlp20-induced priming[29], indicating that PAD4 may play a more significant role in both ETI- and PTI-primed disease resistance than SAG101 in Arabidopsis, though both PAD4 and SAG101 are required for the disease priming of TNL-mediated ETI.

We further tested ETI-mediated disease priming with SETI_*ngr1s* and SETI_*adr1s* mutants and the higher-order SETI_*helperless* mutant, referring to as a quintuple mutant with the loss-of-function of both *adr1s* and *nrg1s*, *adr1 adr1-l1 adr1-l2 nrg1a nrg1b*[15,17]. E2-pretreated SETI_*nrg1s* show no significant defects in disease priming, which is similar to SETI_wt and SETI_*sag101*, whereas SETI_*adr1s* resembles the phenotype of SETI_*pad4* (**Figure S4**). A complete loss in disease priming is only observed in E2-pretreated SETI_*helperless* plants, and together with the results from SETI_*ps* (**Figure 3**, **S4**), it can be inferred that both PAD4-ADR1 and SAG101-NRG1 nodes are required for TNL-activated ETI-mediated immune priming.

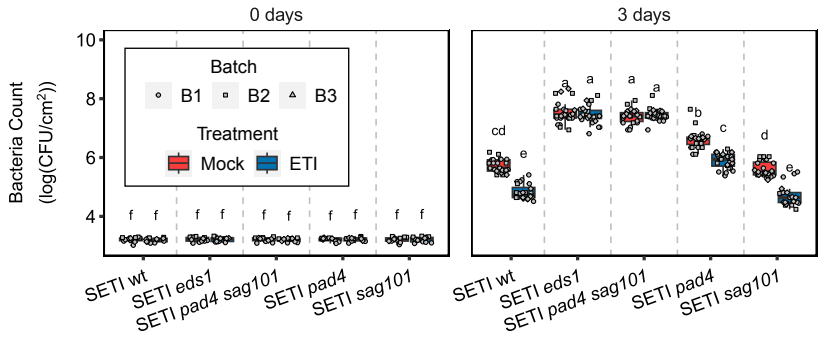

Figure 3. ETI-directed disease priming in SETI lipase-like protein mutants. Indicated mutants of lipase-like proteins were infiltrated with E2 or mock one day before infiltration with *Pst* DC3000 EV. Bacterial CFU were counted at day '0' and day '3' after infiltration with DC3000 EV. Letters showing statistical differences (Tuckey-HSD-Test, $p \leq 0.05$).

ETI-specific defense gene profiling mediated by PAD4-ADR1s and SAG101-NRG1s

We performed genome-wide RNA-seq on SETI mutant lines by specifically inducing ETI through E2 treatment to investigate the differences and similarities of defense gene activation between SAG101-NRG1s and PAD4-ADR1s nodes. We found 5067 differentially expressed genes (DEGs) across all tested genotypes and treatments with *p*-value < 0.01 and |log2[fold change (FC)]| ≥ 1 (**Figure 4**, **Tables S1-S11**). There are 1,902 up-regulated genes in the SETI_wt, 1,707 up-regulated genes in the SETI_*pad4*, and 2,281 up-regulated genes in the SETI_*sag101* E2-treated samples compared to mock-treated samples (**Figure S5B**). The DEGs post E2-treatment, both upregulated and downregulated, are substantially reduced in the SETI_*pad4* mutant compared to the SETI_wt plants (**Figure S5A, S5B**), indicating that PAD4 plays a major role in TNL-mediated ETI-induced transcriptional reprogramming and its loss-of-function could not be compensated by SAG101. Conversely, this reduction in DEGs number is not observed in the SETI_*sag101*. Instead, more

DEGs are found in SETI_*sag101* compared to SETI_wt, which might be due to overcompensation by functional PAD4 or by another unknown mechanism of synergy between PAD4 and SAG101. The persistence of DEGs in the SETI_*sag101* mutant indicates that SAG101 may not be as critical as PAD4 in suppressing or modulating these gene expressions during ETI early activation. This differential impact on gene expression between the two mutants highlights a divergent role of PAD4 and SAG101 in the plant immune response, emphasising the complexity of ETI signalling pathways. These results also highlight the unequal redundancy between PAD4-ADR1s and SAG101-NRG1s, consistent with previous reports that ADR1s can compensate for NRG1s but not *vice versa*[17]. There are no DEGs in SETI_*eds1* and SETI_*pad4 sag101* after E2 treatment compared to mock, demonstrating that *eds1* mutant and *pad4 sag101* double mutant can completely block the TNL-mediated ETI-specific transcriptional reprogramming.

Hierarchical clustering of the DEGs in the heat map revealed 10 clusters using a Euclidean distance and ward.D clustering algorithm (**Figure 4**)[30]. Clusters 3, 5, 6, 7, 8, and 9 show defense-related DEGs according to the gene ontology (GO) analysis from g:Profiler (FDR < 0.05, Benjamini-Hochberg) indicating that these are immune-related clusters (**Figure 4**). The well-known immune-related genes from each cluster and their expression patterns across the SETI mutants were highlighted (**Figure 4**, **Table S1**). Among the immune clusters, cluster 5 comprises genes such as the N-hydroxy pipecolic acid (NHP) biosynthetic genes *FLAVIN-DEPENDENT MONOOXYGENASE* (*FMO1*) and *AGD2-LIKE DEFENSE RESPONSE PROTEIN 1* (*ALD1*)[31], while clusters 5 and 9 contains genes related to cell death. On the other hand, cluster 7 includes genes mainly associated with salicylic acid biosynthesis and signalling, like *ISOCHORISMATE SYNTHASE 1* (*ICS1*), *ENHANCED DISEASE*

SUSCEPTIBILITY 5 (*EDS5*), and *NONEXPRESSOR OF PATHOGENESIS-RELATED GENES 1* (*NPR1*)[32]. Cluster 8 contains genes related to jasmonate signalling. We further extended our analysis on the downregulated DEGs in clusters 1, 2, 4, and 10, predominantly composed of downregulated genes during ETI early activation. GO term analysis of these clusters revealed that most GO terms are related to hormone response, sugar biosynthesis, sugar metabolism, and developmental and photosynthetic pathways (**Figure S5C, S5D, S5E, S5F**). This indicates a significant negative influence of ETI activation on specific plant hormonal, cellular, and metabolic processes, aligning with earlier studies[33]. The constitutive effects of this negative influence might be one of contributing factors to the severe growth retardation of SETI_wt and SETI_*sag101* on E2 plates. We also examined the expression profiles of the genes enriched in selected GO terms (**Figure S6**). Interestingly, the downregulation patterns in SETI_wt and SETI_*sag101* are quite similar, whereas SETI_*pad4* shows a less pronounced downregulation in a majority of genes related to carbohydrate metabolism, plant morphogenesis, and photosynthesis to some extent (**Figure S6**). In addition, similar trends were observed concerning hormone pathway genes, including auxin response genes, which play an integral role in lateral root formation[34]. These findings provide some initial indications that might explain the partial elevation in growth arrest and lateral root formation observed in SETI_*pad4* plants.

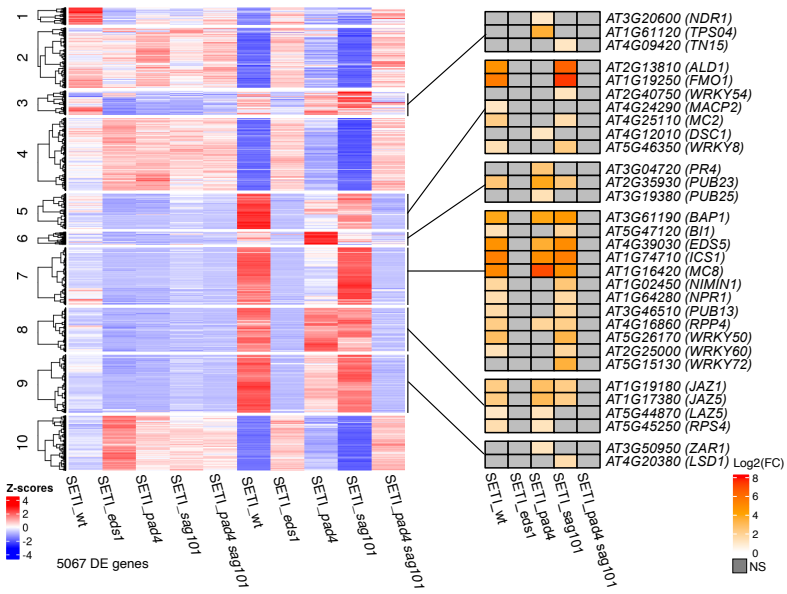

Figure 4. Analysis of TNL-dependent transcriptional changes across SETI lipase-like protein mutants. Five- to six-week-old SETI_wt, SETI_*eds1*, SETI_*pad4*, SETI_*sag101*, and SETI_*pad4 sag101* plants were infiltrated with mock (10 mM $MgCl_2$), and 50 µM E2 (ETI). Samples were collected at 4 h post infiltration (4 hpi) for RNA-seq analysis. The left heatmap shows the normalised expression z-score of all the differently expressed genes with a false discovery rate (FDR) of $p < 0.01$ and a fold change of ≥ 1. No significant gene expression changes in SETI_*eds1* and SETI_*ps* after ETI-treatment induction. SETI_wt, SETI_*pad4*, and SETI_*sag101* show visible expression after ETI-treatment induction. The right heat map represents the expression pattern of key immune genes from each immunity-related cluster among the SETI lipase-like protein mutants i.e. SETI_wt, SETI_*pad4*, and SETI_*sag101*.

Defining the specificity of PAD4 and SAG101-mediated transcriptional reprogramming

The upregulated DEGs were further classified into PAD4- and SAG101-dependent and shared DEGs (**Figure 5A**, **Table S15**). A total of 438 DEGs

were identified as PAD4-dependent, as they were upregulated in both SETI_wt and SETI_*sag101* but downregulated or showed no significant difference in SETI_*pad4*. Similarly, 85 DEGs were classified as SAG101-dependent, being upregulated in SETI_wt and SETI_*pad4* but downregulated or showing no significant difference in SETI_*sag101* (**Figure 5A**). Additionally, 121 DEGs showed shared dependency on both PAD4 and SAG101. Furthermore, 1,258 DEGs were upregulated in SETI_wt, SETI_*pad4*, and SETI_*sag101,* indicating that the transcriptional regulation of these DEGs is ETI-specific but redundantly regulated by PAD4 and SAG101 (**Figure 5A**, **S7A-S7C**). These 1,258 genes were further classified based on partial dependency on PAD4, SAG101, or both (**Table 1**, **Table S16**). GO term analysis of these genes was performed, highlighting those associated with immune-related biological functions (**Figure 5B-5D**, **Table S12-S14**). Interestingly, more DEGs were PAD4-dependent than SAG101-dependent (**Figure 5B**, **5C**). Some genes related to SAR, such as *FMO1* and *ALD1*, were exclusively dependent on PAD4, while other genes showed dependency on both PAD4 and SAG101 (**Figure 4, 5B, 5D**; **Table S12, S14**).

Table 1. Classification of up-regulated genes into partially PAD4-dependent, partially SAG101-dependent, and PAD4/SAG101-dependent categories. *1: DEGs present in SETI_wt, SETI_*pad4*, and SETI_*sag101*. However, in partially PAD4-dependent DEGs the $\log_2$ fold change (FC) difference between SETI and SETI_*pad4* is greater than 1, but there is no $\log_2$ FC difference between SETI_wt and SETI_*sag101*; In partially SAG101-dependent DEGs the $\log_2$ FC difference between SETI_wt and SETI_*sag101* is greater than 1, but no difference between SETI_wt and SETI_*pad4*. *2: DEGs present in SETI_wt, SETI_*pad4* and SETI_*sag101*. The $\log_2$ FC between SETI_wt and SETI_*pad4* and SETI_wt and SETI_*sag101* differ at a magnitude of at least 1.

Categories	DEGs numbers
DEGs partially dependent on *PAD4*[*1]	192
DEGs partially dependent on *SAG101*[*1]	80
DEGs dependent on both *PAD4* and *SAG101*[*2]	64

It is evident from the ion leakage data that SAG101 contributes more to cell death, but PAD4 has synergistic effects in addition to regulating cell death. As expected, cell-death-related genes were found in all categories, including PAD4-specific, SAG101-specific, and PAD4/SAG101-shared. For instance, genes enriched in cell death-related GO terms such as *METACASPASE 2* (*MC2*), *MC8*, *CYSTEINE-RICH RECEPTOR-LIKE KINASE 13* (*CRK13*), *BAX INHIBITOR 1* (*BI1*) are found to be dependent on PAD4 (**Figure 5B**, **Table S12**). On the other hand, genes like *LAZARUS 5* (*LAZ5*) and *CRK4* are dependent on SAG101 (**Figure 5C**, **Table S13**), while *BCL-2 ASSOCIATED ATHANOGENE 6* (*BAG6*) and *MEMBRANE ATTACK COMPLEX/PERFORIN-LIKE 2* (*MACP2*) depend on both PAD4 and SAG101 (**Figure 5C**, **Table S14**). Similar observations were made with the downregulated DEGs, with some DEGs being shared and others exclusively regulated by PAD4 or SAG101 (**Figure S5A**, **Table S18**).

Collectively, these findings highlight the redundant regulation of transcriptional reprogramming by PAD4 and SAG101, demonstrating that while some DEGs are uniquely controlled by one node, a significant portion is co-regulated by both, underscoring their unequal redundant roles in orchestrating the ETI response. In summary, PAD4 seems to play a prominent role in regulating ETI-activated transcriptional reprogramming compared to SAG101, which may explain why PAD4 contributes more to the ETI-induced growth arrest and immune priming, whereas SAG101

plays a more prominent role in cell death. It still needs to be determined how the specificity of transcriptional regulation is achieved by these two unequally redundant nodes downstream of ETI mediated by TNLs.

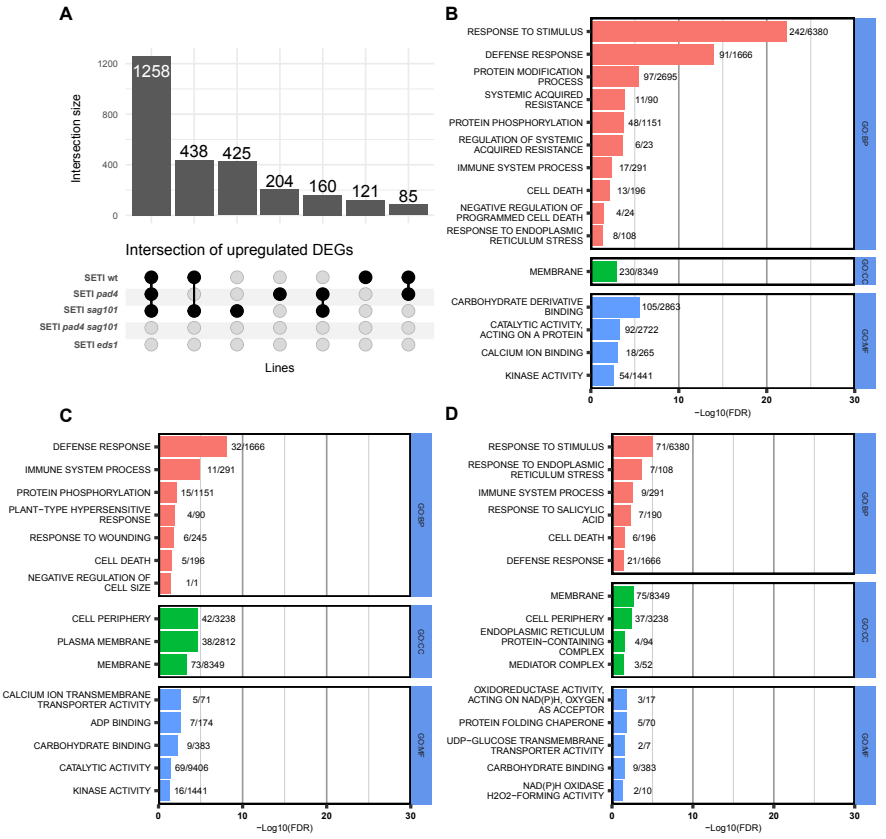

Figure 5. **Comparison of gene up-regulation in ETI treatments across lipase-like protein mutants**. A. Up-Set plot shows 1258 DEGs affected by both PAD4 and SAG101. 438 DEGs are *PAD4*-dependent, and 85 DEGs are SAG101-dependent. B. GO enrichment for PAD4-dependent DEGs. C. GO enrichment for SAG101-dependent DEGs. D. GO enrichment for PAD4/SAG101-shared DEGs. GO analysis is done with g:Profiler, and the GO terms were shown in different enrichment analyses, including biological process (GO:BP), cell components (GO:CC), and molecular function (GO:MF) (FDR ≤ 0.05, Benjamini-Hochberg).

Discussion

EDS1 interacts with either of two other lipase-like proteins, PAD4 and SAG101, to initiate the ETI downstream signalling after sensor TNL activation[8,35,36]. Upon TNL activation, helper NLRs ADR1 or NRG1 interact with the EDS1-PAD4 and EDS1-SAG101 modules, respectively[16]. ETI promotes interaction between NRG1 and EDS1/SAG101 but NRG1/EDS1/SAG101 oligomerization requires PTI[19,37,38]. EDS1-PAD4-ADR1s and EDS1-SAG101-NRG1s have been shown to play unequally redundant roles in plant immune responses[16,17]. EDS1/PAD4/ADR1s contribute more to disease resistance, while EDS1/SAG101/NRG1s, contribute more towards cell death. However, the downstream components and the molecular machinery underlying the unequal roles are still poorly understood.

Here, we focused on investigating ETI-specific roles of the PAD4 and SAG101 nodes. We use the mutants of EDS1 family proteins and helper NLRs in an inducible ETI genetic background to determine the involvement of these proteins in mediating ETI-specific signalling. A partial relief of growth reduction, as well as of inhibition in the lateral root, was observed in SETI_*pad4* compared to SETI_*sag101* on E2 plates, indicating that PAD4 plays an important role in coordinating the balance between growth, development, and defense[23]. SAG101 also synergises with PAD4 in the growth-defense trade-off, as only the SETI_*ps* double mutant shows no growth inhibition. As the detailed mechanisms of growth-defense trade-off remain unexplored, our report regarding the differential roles of PAD4 and SAG101 in mediating ETI-specific growth inhibition provides additional information to help decipher the underlying molecular mechanisms.

We define immune priming as being the strengthening of plant disease resistance after subjecting plants to a priming treatment. Here, we show

that SETI_*pad4* (similarly SETI_*adr1s*) and SETI_*sag101* (similarly SETI_*nrg1s*) both show some immune priming upon ETI activation, though both *pad4* (or *adr1s* triple mutant) and *sag101* (or *nrg1s* double mutant) plants are more disease susceptible[14,16]. These indicate that plants with partially compromised immunity still retain priming capacity for disease resistance. This insight could support improved agricultural practices. For instance, for emerging or remerging pathogens that can partially escape from the immune surveillance system or dampen the immune activation process, one can test whether ETI-mediated immune priming can enhance crop disease resistance. Here, we have only explored the short-term priming capacity in such mutants, and priming could provide longer-term protection. Therefore, it will be interesting to investigate the persistence of this immune memory and how this priming effect has been 'memorised' or 'imprinted' inside plant cells.

Previous studies have elucidated that HR and disease resistance mechanisms can operate independently[39]. Extending this understanding, our analysis shows that the SAG101-NRG1s module predominantly facilitates ETI-activated cell death, while the PAD4-ADR1s module is more critical for initiating disease resistance. Despite this specificity, both modules have overlapped functions in regulating HR and resistance, though in partially redundant roles. Specifically, NRG1s are required for TNL-mediated disease resistance to obligate biotrophic oomycete pathogens, including the downy mildew agent *Hyaloperonospora arabidopsidis* (*Hpa*) and the white rust causative *Albugo candida*[14]. ADR1s are also required for TNL-mediated resistance against *Hpa*[12]. While the *sag101* single mutant exhibits only isolated single-cell HR cell death, which appears to confer a less severe susceptibility than the *nrg1a nrg1b* double mutant, both SAG101 and NRG1s are consistently implicated as part of the same downstream signalling pathway mediated

by EDS1 in multiple instances[14–16,40]. The *pad4* single mutant can produce conidiospores accompanied by single-cell trailing necrosis, which aligns with that observed in the *adr1s* triple mutant[40,41]. More intriguingly, SAG101 and NRG1s appear dispensable for conferring resistance against the hemibiotrophic bacterial pathogen *P. syringae*, where the PAD4-ADR1s node assumes a more important role. Therefore, it is imperative for future studies to comprehensively evaluate disease resistance across a range of mutants, including those carrying mutations in lipase-like protein-encoding genes (*pad4*, *sag101*, and their double mutant), as well as those affecting hNLR-encoding genes (*nrg1s*, *adr1s*, and their quintuple *helperless* mutant). It is also crucial to expand testing their responses to more different types of plant pathogens. Furthermore, it is key to investigate further how each node modulates the functional preference towards HR and resistance and how these are linked to the differential phenotypes of ETI-induced growth inhibition and disease priming. In addition, it will provide valuable insights into NLR-mediated immune effectiveness to explore how the synergistic effects of SAG101-NRG1s and PAD4-ADR1s nodes are achieved.

Importantly, ETI is always preceded by PTI in authentic interactions with microbes, making it challenging to study ETI-specific responses. For instance, in the heat map that encompasses all the treatments (PTI, ETI, 'PTI+ETI'), gene expression patterns in 'PTI+ETI' are much less distinguishable across different lipase-like mutants compared to those in the ETI-only treatment (**Figure S8**). We suspect that PTI can potentially mask the overall ETI transcriptome by pre-emptively activating a set of defense-related pathways that overlap with those induced during ETI. Specifically, PTI-induced genes may saturate the cellular response machinery, thereby attenuating or obscuring the subsequent activation of ETI-specific genes. This is supported by the observation that, in SETI_wt,

ETI activates a distinct set of genes that are not revealed in combined PTI+ETI treatment, via the analysis of DEGs across all conditions (PTI, ETI, and PTI+ETI) (**Figure S9**, **Table S17**). This observation reinforces the value of examining ETI in isolation to identify its unique contributions to gene regulation. In addition, a considerable reduction in the number of upregulated genes in PTI+ETI treatment is observed compared to ETI treatment alone. This suggests that PTI treatment may lead to the expression of specific genes reaching a threshold that renders subsequent responses to ETI less pronounced. This masking effect might explain why the PTI and PTI+ETI profiles appear similar in our heatmap (**Figure S8**). Moreover, the choice of using the 4 hours post infiltration (hpi) time point might have contributed to this observation. This time point is relatively late for capturing early PTI responses[42] but still within the window where downstream ETI effects could manifest. It's plausible that at this stage, some responses typically associated with ETI could be acting synergistically with PTI, especially since the bacteria utilised have a functional Type III Secretion System. We also found similar effects in several recent reports[17,43]. TNLs or TIR-only proteins possess enzymatic activities to produce small molecules that associate with different EDS1 complexes with either PAD4-ADR1s or SAG101-NRG1s[44]. Our transcriptome profiling results for either PAD4-ADR1s or SAG101-NRG1s modules specific to ETI might provide additional insights. It has been shown that EDS1-SAG101-NRG1s hNLR resistosome formation requires the cell-surface immune receptor-mediated PTI; it would be interesting to compare the gene expression patterns between PTI, ETI, and 'PTI+ETI' in SETI_*pad4*. A few other important unresolved questions remain: How do the resistosomes formed by NRG1s and ADR1s activate ETI downstream responses? Are the cation channel activities of NRG1s and ADR1s sufficient to activate the observed transcriptional reprogramming?

More broadly, it has been reported that PAD4 and SAG101 from different plant species may have various functions during TNL-mediated ETI activation. For instance, the Solanaceae genome mainly encodes two SAG101 isoforms (SAG101a, SAG101b), and EDS1-SAG101b has been shown to play a crucial and sufficient role in nearly all TNL-mediated ETI immune responses in *Nicotiana benthamiana* (*Nb*). In contrast, *Nb*PAD4 did not show any significant roles[36]. However, similar to *Nb*SAG101s, *Nb*NRG1 is important in regulating ETI downstream of EDS1 in *Nb*[37,45]. Conceivably, the EDS1-SAG101-NRG1 node plays a crucial role in regulating both disease resistance and cell death in *Nb*, while in contrast, EDS1-SAG101-NRG1 in Arabidopsis is more specialised to HR. It will be interesting in the future to generate ETI-inducible lines in *Nb* that are similar to SETI in Arabidopsis, to study ETI-specific responses mediated by *Nb*PAD4 and *Nb*SAG101 to dissect the ETI-specific downstream signalling in comparison to those in Arabidopsis, which may provide more insights in ETI-mediated growth-defense trade-off and immune priming. In summary, our studies have provided valuable datasets to dissect modular mechanisms of immune priming and growth inhibition mediated by ETI, which could underpin more innovative plant breeding for disease resistance.

Acknowledgements

We thank Marc Gebauer for their technical assistance with the genotyping of mutants and Ewout van Diepen for their invaluable help during the more labour-intensive aspects of our experimentation. Their contributions were instrumental to the successful completion of this work. HC, HHN, PY and PD acknowledge a European Research Council Starting Grant 'R-ELEVATION' (grant agreement: 101039824). JDGJ was supported by the Gatsby Foundation (United Kingdom).

We sincerely thank the readers of our initial preprint for their valuable feedback and for pointing out errors. We have incorporated these corrections into this second version. We welcome any further suggestions or comments that can help us improve our manuscript.

Competing interests

The authors declare no competing interests.

Author contributions

PD conceptualised and oversaw the inception of the research project. The experimental work was collaboratively conducted by PD, HC, and PY. Data analysis and figure generation were performed by HC, HHN, PY and PD. JDGJ was involved throughout the project, providing valuable discussions that significantly shaped the research. HC and PD wrote the initial manuscript draft. All co-authors contributed to subsequent revisions and editorial processes. The final manuscript was prepared by HC and PD and was approved for submission by all authors.

Data and code availability

- The RNA-seq data for this study have been deposited in the European Nucleotide Archive (ENA) at EMBL-EBI under accession number: PRJEB62154.
- All codes are available via GitHub: https://github.com/dinglab-plants/ETI_Project and deposited in Zenodo under https://doi.org/10.5281/zenodo.14673399.

Material and Methods

Plant material and growth conditions

Arabidopsis thaliana accessions Col-0 and a β-estradiol (E2) inducible Super-ETI line (SETI_wt), were used as the wild-type controls in this study. The lipase-like mutants SETI *eds1-2* (SETI_*eds1*), SETI *pad4-1* (SETI_*pad4*), SETI *sag101-1* (SETI_*sag101*), and SETI *pad4-1 sag101-*

1 (SETI_*ps*) and helper NLR mutants, including SETI *adr1-1 adr1-L1 adr1-L2 nrg1a nrg1b* (SETI_*helplerless*), SETI *nrg1a nrg1b* (SETI_*nrg1s*), and SETI *adr1-1 adr1-L1 adr1-L2* (SETI_*adr1s*) are generated by crossing all the previously reported mutants with SETI plants[12,14,40].

For square and round plate assay, seeds were processed by liquid sterilization (70% ethanol 5 minutes, bleach solution 5 minutes, 100% ethanol 5 minutes, washed three times with sterilized water, and soaked into 0.5% agarose in 4 °C dark condition for one day). Seeds were sown on a 9 cm petri dish or square petri dish (120 mm x 120 mm), GM (Germination media) plate, or GM plate with 50 μM of E2. For square plates 1.2% agarose was used while for circular plates 0.8% agarose was used. Plants were grown at 21 °C under long-day conditions (16 h light, 8 h dark), and at 50% humidity. Photos were taken 14 and 18 days after sowing. Col-0 was used as the negative and SETI as the positive control.

Bacterial strains and growth conditions

The various bacteria strains used in this study were described in the Key Resources Table. *Pseudomonas syringae* pv. tomato (*Pst*) DC3000 EV (carrying empty vector) grown on the King's B medium plates 25 μg mL^{-1} rifampicin, and 50 μg mL^{-1} kanamycin and *Pst* DC3000 *hrcC*$^{-}$ were grown on the King's B medium plates 25 μg mL^{-1} rifampicin. *Pseudomonas fluorescens* engineered with a Type III secretion system (Pf0-1 'EtHAn' strains) expressing empty vector was grown on the King's B medium plates with. All the Pseudomonas strains were grown on plates at 28°C for 2 days for further inoculum preparation.

Fresh weight measurement

The seeds were processed by liquid sterilization and sown on a square petri dish, GM plate, or GM plate with 50 μM of E2 for 18 days. Six seedlings were pooled together to measure the fresh weight. All statistics

and figures are generated in R version 4.3.1. ANOVA (p- value ≤ 0.05) was used for identifying significant factors. A least significant difference (LSD) test (p-value ≤ 0.05) was used to identify differences between treatment and lines. A detailed statistical summary is available on GitHub: https://github.com/dinglab-plants/ETI_Project.

RNA-seq raw data processing, alignment, quantification of expression, and data visualization

DMSO in 10 mM $MgCl_2$, 50 µM E2 in 10 mM $MgCl_2$, *Pseudomonas fluorescens* (Pf0-1)[46] in 10 mM $MgCl_2$, or Pf0-1 and 50 µM E2 in 10 mM $MgCl_2$ was infiltrated in 5 to 6-week-old Arabidopsis leaves with 1 mL needleless syringe for RNA-seq sample collection. Two leaves per sample were collected at 0 and 4 hpi as 1 biological replicate. RNA was extracted with the Zymo RNA extraction kit[47].

The RNA sample was sequenced by Novogene. Raw reads were trimmed into 390 bp clean reads by the Novogene bioinformatics service. At least 12 million paired-end clean reads for each sample were provided by Novogene for RNA-seq analysis. All reads passed FastQC before the following analyses[48]. All clean reads were mapped either to the TAIR10 Arabidopsis genome/transcriptome via TopHat2 or to a comprehensive Reference Transcript Dataset for Arabidopsis Quantification of Alternatively Spliced Isoforms (AtRTD2_QUASI) containing 82,190 non-redundant transcripts from 34,212 genes via Galaxy and Salmon tools[49,50]. The estimated gene transcript counts were used for differential gene expression analysis and statistical analysis with the 3D RNA-seq software[51]. The low-expressed transcripts were filtered if they did not meet the criteria of ≥3 samples with ≥1 count per million reads. The batch effects between three biological replicates were removed to reduce artificial variance with the RUVSeq method[52]. The expression data were normalised across samples with the TMM (weighted trimmed mean of M-

values)[53]. The significance of expression changes in the contrasting groups 'SETI_wt_ETI vs SETI_wt_mock', groups 'SETI_*eds1*_ETI vs SETI_wt_mock', 'SETI_*pad4*_ETI vs SETI_wt_mock', 'SETI_*sag101*_ETI vs SETI_wt_mock' and 'SETI_*ps*_ETI vs SETI_wt_mock' were determined by the limma-voom method[54,55]. A gene was defined as a significant differentially expressed gene (DEG) if it had a Benjamini–Hochberg adjusted *p*-value < 0.01 and log2[fold change (FC)] ≥ 1 (upregulated) or log2[fold change (FC)] ≤ -1 (downregulated). The GO term analysis was analysed with g:Profiler[56].

Electrolyte leakage assay

Two leaves of 5-week-old Arabidopsis plants were hand infiltrated using a 1 mL needleless syringe with 50 µM E2 dissolved in Mili-Q water or DMSO in Mili-Q water as mock. Leaf discs were collected with a 7-mm diameter cork borer from infiltrated leaves on paper towels. Leaf discs were dried and transferred into 2 mL of deionised water in 12-well plates (2 leaf disks per well. The plate was incubated for 30 minutes in a growth chamber with controlled conditions at 21 °C under long-day conditions (16-h light/8-h dark) with a light intensity of 120-150 µmol m^{-2}. The water was replaced after incubation with 2 mL of deionised water. Electrolyte leakage was measured with Pocket Water Quality Meters (LAQUAtwin-EC-33; Horiba) calibrated at 1.41 mS/cm. Around 100 µL of the sample was used to measure conductivity at the indicated time points. ANOVA (*p*-value ≤ 0.05) was used for identifying significant factors. Tukey-HSD-Test (*p*- value ≤ 0.05) was used to determine differences between treatment and lines. A detailed statistical summary is available on GitHub: https://github.com/dinglab-plants/ETI_Project.

Semi-quantitative real time-PCR

Complementary DNAs (cDNAs) were synthesised from the RNA extracted for RNA-seq from SETI_wt and all lipase mutants in SETI background

using a first-strand cDNA synthesis kit (Thermo Scientific) according to the manufacturer's instructions. 1 µL of cDNA was combined in a 15 µL reaction with 3mM dNTP, 2µM of each primer, 10xPCR buffer and Milli Q water. Semi-quantitative real-time-PCR (RT-PCR) analysis was performed using *AvrRps4* specific primers (*AvrRps4_F*: 5'-TCCAGCTTCAGTTACTCGGC-3'; *AvrRps4*_R: 5'-TTGGCTATTTCGGCTGGGTT-3'). The elongation factor 1α (*EF1α*) primers (*EF1α*_F: 5'-CAGGCTGATTGTGCTGTTCTTA-3'; *EF1α*_R: 5'GTTGTATCCGACCTTCTTCAGG-3') were used as an internal control. The semi-quantitative RT-PCR reaction was performed as follows: pre-denaturation at 94°C (2 minutes), then 35 cycles at 94°C (15 s); 55°C (30 s) and 68°C (1 minute), and a final extension at 68°C for 5 min. The RT-PCR products were electrophoresed and compared on 1.5% TAE agarose gel.

Bacterial growth assay

Pst DC3000 EV (carrying empty vector)[57] was grown on selective King's B (KB) medium plates containing 15% (w/v) agar, 25 µg mL^{-1} rifampicin, and 50 µg mL^{-1} kanamycin for 48 h at 28 °C. Bacteria were harvested and resuspended in 10 mM $MgCl_2$. The concentration of the suspension was adjusted to an optical density of 0.001 at 600 nm [OD_{600}=0.001, representing ~5×10^5 colony-forming units (CFU) mL^{-1}]. Two 5-week-old Arabidopsis leaves were hand infiltrated with 50 µM E2 dissolved in 10 mM $MgCl_2$ or DMSO in 10 mM $MgCl_2$ with a needleless syringe. The following day, the same leaves were infiltrated with bacteria. For quantification, leaf samples were harvested with a 7-mm diameter cork borer, resulting in leaf discs with an area of 0.38 cm^2. Two leaf discs per leaf were collected as a single sample. For each genotype and condition, four samples were collected immediately after infiltration as 'day 0' samples, and eight samples were collected at 3 dpi as 'day 3' samples to

compare the bacterial titres between different genotypes, conditions, and treatments. For 'day 0', samples were ground in 200 µL of 10 mM $MgCl_2$ and spotted (10 µL per spot) on selective KB medium agar plates to grow for 48 h at 28 °C. For 'day 3', samples were ground in 200 µL of infiltration buffer, serially diluted (5, 50, $5x10^2$, $5x10^3$, $5x10^4$, $5x10^5$ times), and spotted (6 µL per spot) on selective King's B medium agar plates to grow for 48 h at 28 °C. The number of colonies (CFU per drop) was counted, and bacterial growth was represented as CFU cm^{-2} of leaf tissue. ANOVA (*p*-value ≤ 0.05) was used for identifying significant factors. Tukey-HSD-Test (*p*-value ≤ 0.05) was used to identify differences between treatment and lines. A detailed statistical summary is available on GitHub: https://github.com/dinglab-plants/ETI_Project.

Chlorophyll content estimation

Two leaves of 5-week-old Arabidopsis plants (SETI_wt, SETI_*eds1*, SETI_*pad4*, SETI_*sag101*, SETI_*ps*, SETI_*adr1s*, SETI_*nrg1s*, and SETI_*helperless*) were hand infiltrated using a 1 mL needleless syringe with 50 µM E2 dissolved in 10 mM $MgCl_2$ as ETI treatment, *Pst* DC3000 *hrcC*$^-$ (0.2 OD)[58] dissolved in 10 mM $MgCl_2$ as PTI treatment, E2+*Pst* DC3000 *hrcC*$^-$ with same concentration as 'PTI+ETI' treatment and DMSO dissolved in 10 mM $MgCl_2$ as mock. Leaf disks were collected using a 7-mm diameter cork borer from 3 individual plants as 1 sample for each treatment. Samples were ground and resuspended in 1 mL of 80% acetone. The samples were then centrifuged at 10,000 g for 5 mins. The absorbance of the supernatant was measured at 645 nm and 633 nm using UV–VIS spectrophotometer (UV-6300PC, VWR). Total and chlorophyll a, b content were calculated according to the following equations[59]:

Chl-a = 12.72A663-2.59A645/1000 mg per g FW (mg g^{-1})

Chl-b = 22.9A645 -4.67A663/1000 mg per g FW (mg g^{-1})

Chl-t= 20.31 A645 +8.05 A663/1000 mg per g FW (mg g^{-1})

ANOVA (p-value ≤ 0.05) was used for identifying significant factors. Tukey-HSD-Test (p-value ≤ 0.05) was used to identify differences between treatment and lines. A detailed statistical summary is available on GitHub: https://github.com/dinglab-plants/ETI_Project.

Quantification and statistical analysis

R version 4.3.1 was used for data analysis. Boxplots and bar plots were generated using ggplot2. The heatmap on the right side in **figure 4** was generated with the R package 'ComplexHeatmap'[60]. The upset plot and the volcano plot were generated with the R packages 'ComplexUpset'[61] and 'EnhancedVolcano'[62]. **Figure S6** was done with 'gt'[63] and 'gtExtras'[64]. The following packages were used for data formatting and statistics: 'Tidyverse'[65], 'multcompView'[66], 'agricolae'[67], 'ggpubr'[68], 'stringr'[69], 'r2r'[70] and 'circlize'[71]. RNA-seq analysis was done as described above.

Supplementary information

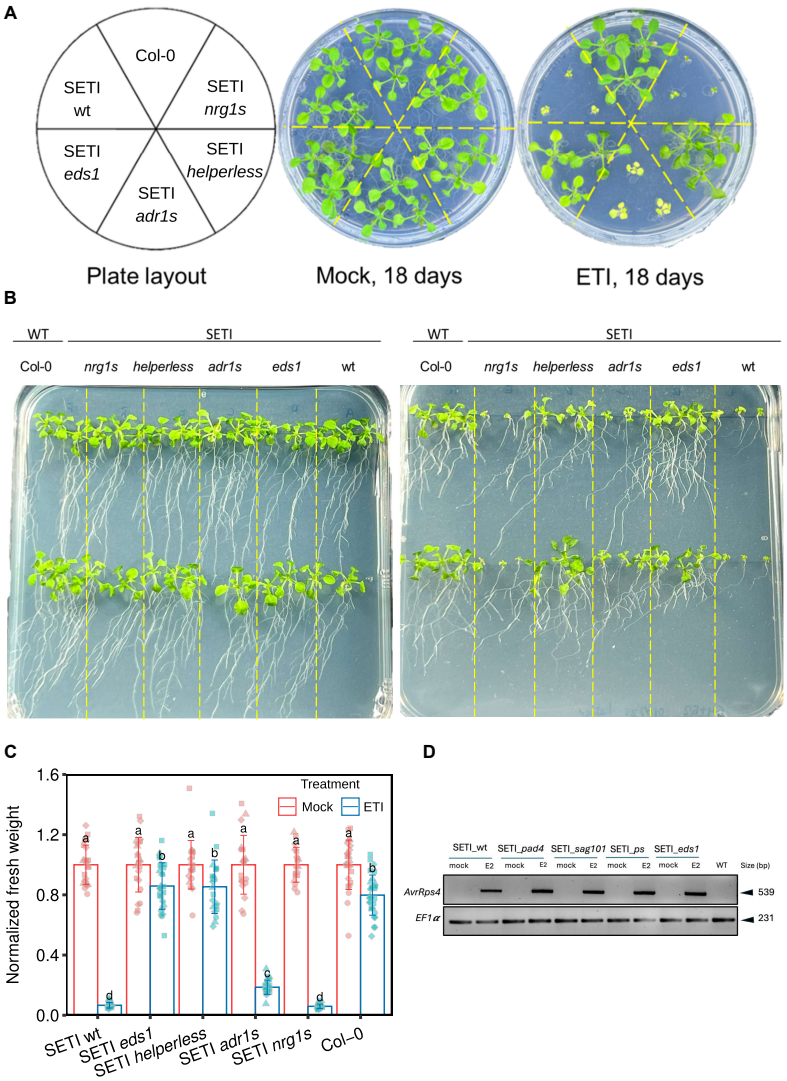

Figure S1. Estradiol induced growth arrest phenotype in helper NLR mutants. Related to Figure 1. A. Indicated mutants of helper-NLRs (SETI_wt, SETI_*nrg1s*, SETI_*adr1s* and SETI_*helperless*, SETI_*eds1*) were sown on round plates with or without E2 (50 µM), and their growth

arrest phenotypes were observed 18 days after planting on E2 plates. B. Indicated helper-NLR mutants were sown on square plates with or without E2 (50 µM) and were grown vertically. Growth arrest and lateral root formation phenotypes were recorded 18 days after planting on E2 plates. C. Indicated mutant lines were grown on vertical GM plates with or without E2 (50 µM), and the fresh weight was recorded 18 days after sowing on E2 plates. Fresh weight was normalized to the average fresh weight of the mock controls for the respective lines. The error bars indicate the standard deviation. Letters showing statistical differences (LSD-test, $p \leq 0.05$). D. Semi-quantitative RT-PCR analysis of *AvrRps4* expression in wild-type (SETI_wt) and indicated lipase-like protein mutants (SETI_*sag101*, SETI_*pad4*, SETI_*pad4 sag101*, SETI_*eds1*) compared to Col-0. The upper panel shows PCR amplification of *AvrRps4*, while the lower panel displays PCR products for the *EF1α* housekeeping gene in the same samples, ensuring consistent expression levels across the conditions.

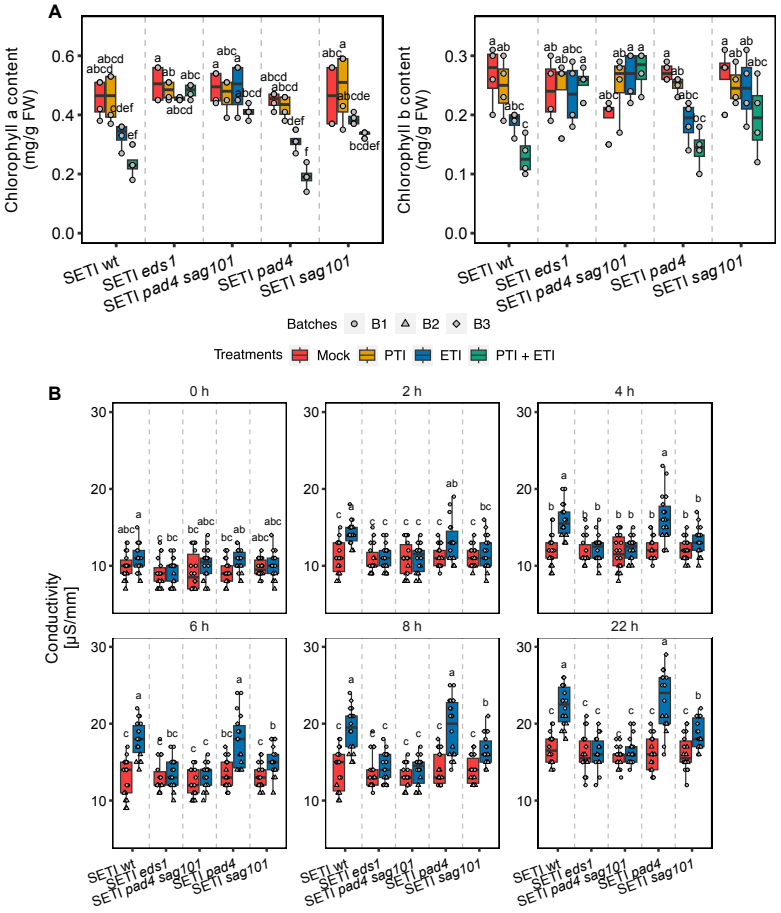

Figure S2. Varying responses of PAD4 and SAG101 modules in ETI-induced cell death. A. SETI lipase-like protein mutants were hand infiltrated with mock, E2 (ETI), E2 + *Pst* DC3000 *hrcC*$^{-}$ (PTI+ETI) and chlorophyll a and b content were recorded 3 dpi. Letters showing statistical differences (Tukey-HSD-Test, *p*-value ≤ 0.05). B. Indicated mutants of lipase-like proteins (SETI_wt, SETI_*sag101*, SETI_*pad4*, SETI_*pad4 sag101*, SETI_*eds1*) were infiltrated with E2 or mock and ion leakage was determined at several timepoints including 0, 2, 4, 6, 8 and 22h. Letters showing statistical differences (Tukey-HSD-Test, $p \leq 0.05$).

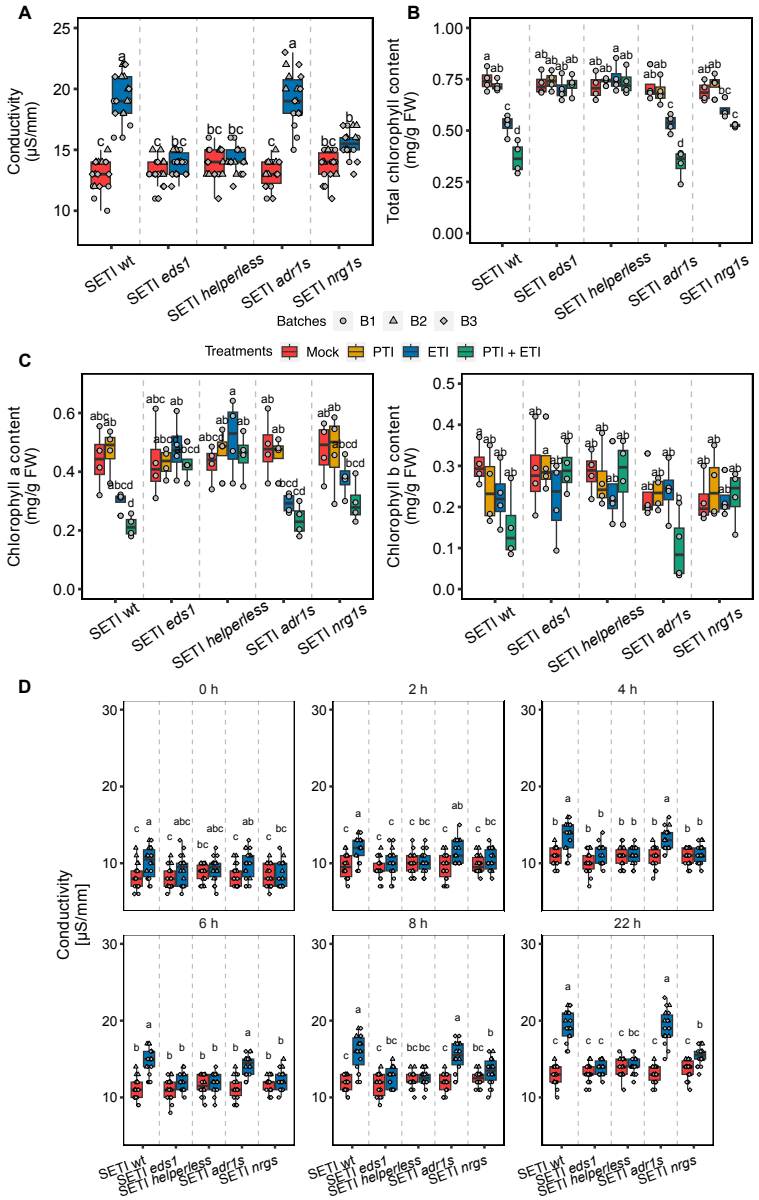

Figure S3. Varying responses of NRG1s and ADR1s modules in ETI-induced cell death. Related to Figure 2. A. Indicated mutant lines of helper-NLRs (SETI_wt, SETI_*nrg1s*, SETI_*adr1s*, SETI_*helperless*,

SETI_*eds1*) in SETI background were infiltrated with E2 or mock and ion leakage was determined at 24 h time point. Letters showing statistical differences (Tukey-HSD-Test, $p \leq 0.05$). B. Total chlorophyll content was estimated on indicated mutants of helper NLRs 3 dpi after E2 infiltration as ETI treatment, *Pst* DC3000 *hrcC*$^-$ as PTI treatment, (E2 + *Pst* DC3000 *hrcC*$^-$) as PTI+ETI treatment and DMSO dissolved in 10 mM $MgCl_2$ as mock. Letters showing statistical differences (Tukey-HSD- Test, $p \leq 0.05$). C. SETI helper-NLR mutants were hand infiltrated with mock, E2 (ETI), E2 + *Pst* DC3000 *hrcC*$^-$ (PTI+ETI) and chlorophyll a and b content were recorded 3 dpi. Letters showing statistical differences (Tukey-HSD-Test, $p \leq 0.05$). D. Indicated mutant lines of helper NLRs (SETI_wt, SETI_*nrg1s*, SETI_*adr1s*, SETI_helperless, SETI_*eds1-2*) in SETI background were infiltrated with E2 or mock and ion leakage was determined at several time points including 0, 2, 4, 6, 8 and 22h. Letters showing statistical differences (Tukey-HSD-Test, $p \leq 0.05$).

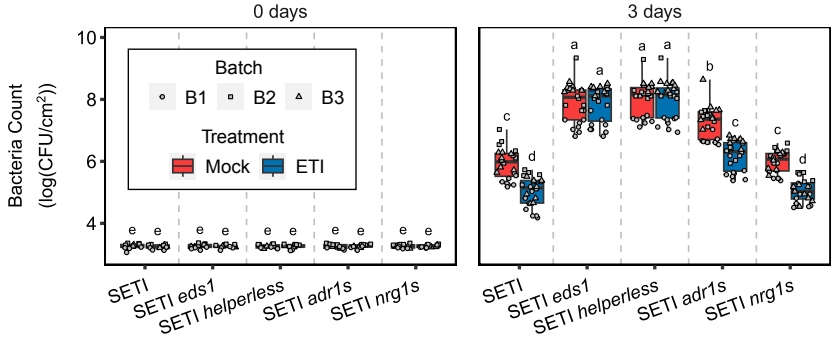

Figure S4. ETI-directed disease priming in SETI helper-NLR mutants. Related to Figure 3. Indicated mutants of helper NLRs were infiltrated with E2 or mock one day before infiltration with Pst DC3000 EV. Bacterial CFU were counted at day '0' and day '3' after infiltration with DC3000 EV. Letters showing statistical differences (Tuckey-HSD-Test, $p \leq 0.05$).

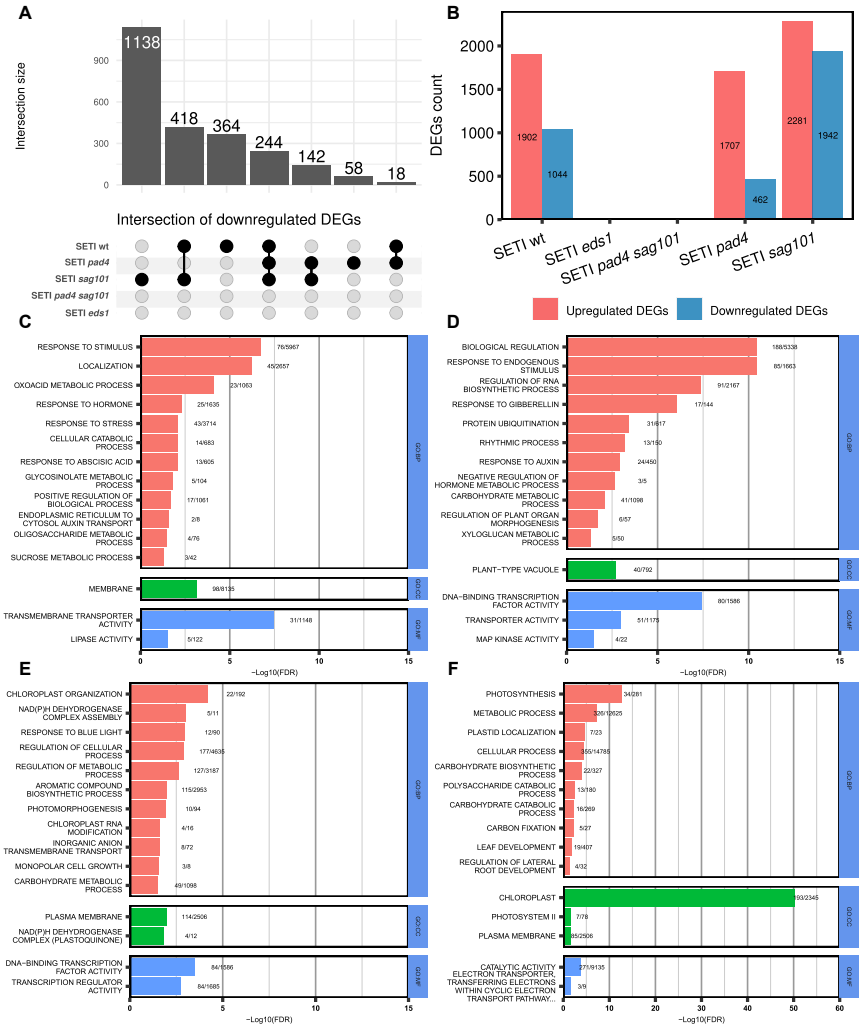

Figure S5. Comparison of gene down-regulation in ETI treatments across lipase-like protein mutants. Related to Figure 4. A. UpSet plot illustrating the intersection sizes of downregulated differentially expressed genes (DEGs) in SETI_wt and SETI lipase-like protein mutants. B. Total number of upregulated and downregulated DEGs across lipase-like protein upon ETI treatment. C. GO enrichment for DEGs in cluster 1 from heatmap in Figure 4, D cluster 2, E cluster 4 and F Cluster 10.

Gene ID	SETI	SETI *pad4*	SETI *sag101*	SETI *pad4 sag101*
Regulation of lateral root development				
AT3G48430	-0.599	-0.398	-1.019	0.234
Photomorphogenesis				
AT4G32980	-1.238	-1.018	-2.641	0.212
AT2G20180	-1.282	-0.924	-1.889	-0.329
AT3G48590	-1.076	-0.867	-1.106	-0.205
AT2G31380	-1.518	-0.852	-1.368	0.051
AT4G08920	-1.096	-0.720	-1.466	-0.178
AT2G36910	-0.701	-0.483	-1.079	-0.047
AT1G69935	-0.498	-0.468	-1.096	0.017
AT2G18790	-0.792	-0.455	-1.006	0.017
AT1G53090	-0.739	-0.425	-1.124	0.231
Leaf development				
AT1G31770	-1.817	-1.607	-2.306	0.336
AT4G25420	-1.106	-0.976	-2.795	-0.099
AT5G04810	-1.049	-0.868	-1.711	0.106
AT1G15690	-0.857	-0.651	-1.756	0.208
AT1G55350	-0.369	-0.330	-1.108	0.108
AT5G55540	-0.434	-0.329	-1.311	0.164
AT3G52910	-2.315	0.176	-2.188	0.310
Photosynthesis				
AT4G25910	-1.078	-0.934	-1.688	0.173
AT3G15095	-1.224	-0.898	-1.772	-0.041
AT5G21930	-0.664	-0.510	-1.517	-0.049
AT1G68890	-0.549	-0.495	-1.566	0.129
AT5G38420	-0.482	-0.479	-1.288	0.096
AT5G01920	-0.479	-0.396	-1.134	0.035
AT4G31390	-0.567	-0.383	-1.209	0.194
AT5G44660	-0.527	-0.309	-1.008	-0.020
Response to gibberellin				
AT2G04240	-1.349	-1.208	-1.547	0.127
AT2G01570	-1.368	-0.876	-1.583	0.062
AT5G67480	-2.336	-0.872	-1.765	-0.024
AT3G47620	-1.623	-0.848	-1.975	0.110
AT3G19100	-1.234	-0.822	-0.991	0.398
AT1G50420	-1.048	-0.627	-1.053	-0.254
AT1G12240	-1.274	-0.580	-1.474	0.158
AT1G66350	-1.563	-0.512	-0.814	0.063
AT4G23060	-1.237	-0.268	-0.944	0.361

Gene ID	SETI	SETI *pad4*	SETI *sag101*	SETI *pad4 sag101*
Regulation of plant organ morphogenesis				
AT5G10150	-1.865	-1.510	-2.318	-0.268
AT2G43010	-1.268	-0.909	-1.328	-0.096
AT1G01030	-1.747	-0.314	-0.387	-0.541
AT3G61460	-1.190	0.206	-0.762	-0.082
Carbohydrate metabolic process				
AT4G36870	-1.337	-0.896	-1.690	0.036
AT2G25450	-1.853	-0.871	-1.504	0.108
AT1G68020	-1.106	-0.756	-0.805	-0.005
AT4G02130	-1.345	-0.728	-1.406	-0.251
AT1G70230	-1.544	-0.689	-1.357	-0.037
AT4G32190	-1.145	-0.683	-1.227	0.290
AT4G17090	-1.438	-0.654	-1.345	0.102
AT2G23760	-1.029	-0.547	-1.437	0.074
AT2G01850	-2.105	-0.521	-1.326	0.026
AT3G62660	-1.205	-0.364	-0.811	0.016
AT1G50460	-1.317	-0.281	-0.596	-0.362
AT1G55850	-1.492	-0.196	-1.494	-0.235
Response to auxin				
AT5G18020	-1.823	-1.543	-3.308	0.089
AT4G34750	-1.293	-0.995	-1.581	-0.351
AT5G67480	-2.336	-0.872	-1.765	-0.024
AT1G12110	-1.418	-0.837	-1.487	-0.226
AT2G28350	-1.685	-0.776	-1.365	-0.115
AT1G12820	-0.983	-0.694	-1.105	-0.064
AT5G47370	-1.735	-0.490	-1.933	0.557
AT2G42580	-1.045	-0.487	-0.497	-0.392
AT2G42620	-0.929	-0.415	-1.168	0.116
AT4G14560	-1.198	-0.401	-1.570	0.399
AT1G75500	-0.890	-0.335	-1.130	-0.177
AT1G22530	-1.498	-0.325	-0.873	-0.066
AT1G19220	-0.940	-0.270	-1.047	0.214
AT1G30330	-1.245	-0.115	-0.583	0.009
AT5G12050	-0.073	0.082	-1.655	-0.291
AT1G19850	-1.193	0.274	-0.091	0.359
AT1G69160	-1.622	0.445	-0.806	0.600
AT1G73590	-0.190	0.487	-1.388	-0.057
Response to abscisic acid				
AT2G35940	-1.528	-0.097	-1.207	0.151

Log$_2$FC

2 to 5
1.5 to 2
1 to 1.5
0.9 to 1
0.8 to 0.9
0.7 to 0.8
0.6 to 0.7
0.5 to 0.6
0.4 to 0.5
0.3 to 0.4
0.2 to 0.3
−0.2 to 0.2
−0.3 to −0.2
−0.4 to −0.3
−0.5 to −0.4
−0.6 to −0.5
−0.7 to −0.6
−0.8 to −0.7
−0.9 to −0.8
−1 to −0.9
−1.5 to −1
−2 to −1.5
−5 to −2

Fig. S6

Figure S6. ETI-induced expression changes in downregulated gene clusters. Related to Figure 4. A Go-term analysis of downregulated DEG cluster 1, 2, 4 and 10 from Figure 4 was conducted and representative GO-terms for each cluster were selected. The log2FC of each DEG from

the selected GO-term categories are listed in the table. Colours are showing the magnitude of the expression change in SETI (SETI_wt), SETI *pad4* (SETI_*pad4*), SETI *sag101* (SETI_*sag101*), and SETI *pad4 sag101* (SETI_*ps*) plants. DEGs and significant Go-terms were defined in the same manner as in Figure 4 and 5.

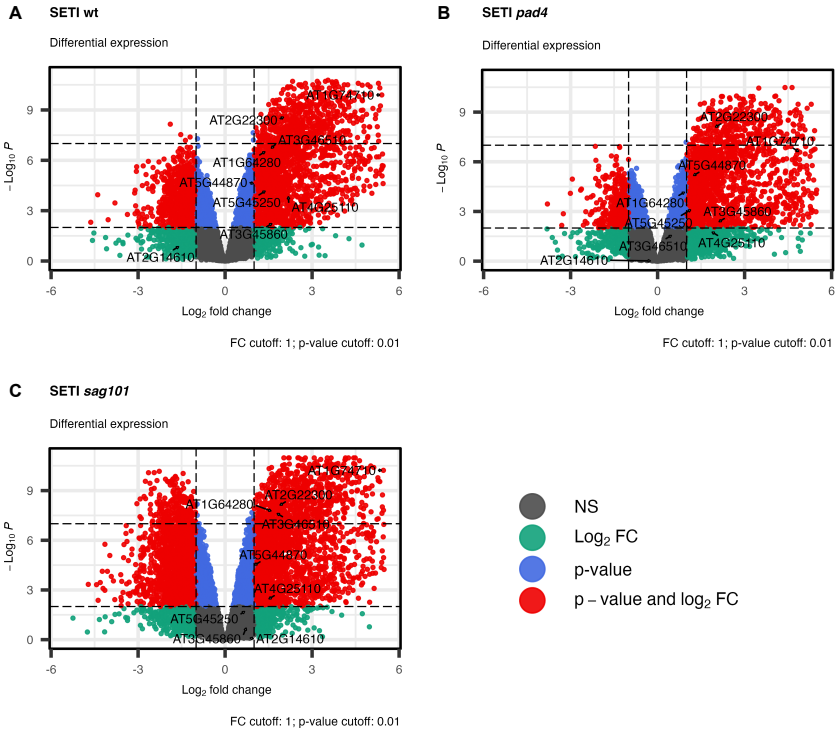

Figure S7. Volcano plot for SETI lipase-like protein mutants. Related to Figure 4. Volcano plot showing expression changes between E2- vs mock-treated samples of SETI_wt plants (A). The gene names of three immune marker genes, three PAD4-dependent genes (B) and three SAG101-dependent genes (C) are highlighted here. Different colours highlighting different thresholds: red ($p \leq 0.01$, $|\log2(FC)| \geq 1$), blue ($p \leq 0.01$, $|\log 2(FC)| < 1$), green ($p > 0.01$, $|\log2(FC)| \geq 1$), and grey ($p > 0.01$, $|\log 2(FC)| < 1$).

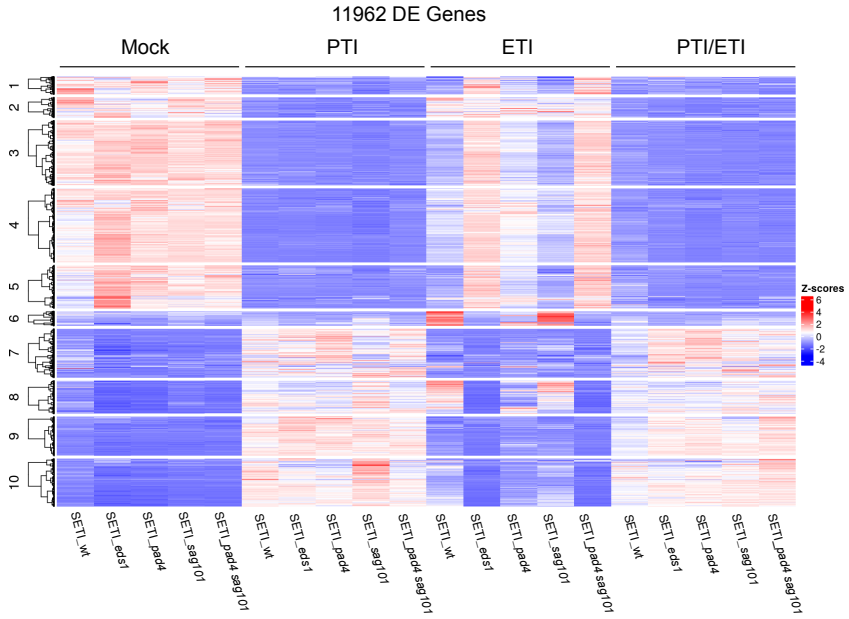

Figure S8. Differential expression profiles of lipase-like protein mutants during immune activation. Related to Figure 4. Five- to six-week-old SETI_wt, SETI_*eds1*, SETI_*pad4*, SETI_*sag101*, and SETI_*pad4 sag101* plants were infiltrated with mock (10 mM $MgCl_2$), PTI (*Pseudomonas fluorescens* (Pf0-1) in 10 mM $MgCl_2$), ETI (50 µM E2 in 10 mM $MgCl_2$), and PTI + ETI respectively. Samples were collected at 4 hours post infiltration (4 hpi) for RNA-seq analysis. The heat map displays the normalized expression (z- scores) of 11,962 differentially expressed genes (DEGs) identified under these conditions across all genotypes. DEGs were filtered based on a false discovery rate (FDR) of $p \leq 0.01$ and a fold change of ≥1.

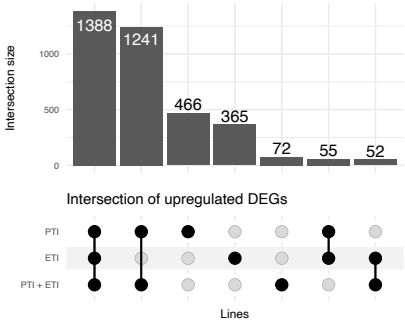

Figure S9. Comparison of gene up-regulation in SETI_wt across PTI, ETI and PTI+ETI treatment. Related to Figure 4-5. The Up-Set plot illustrating the intersection sizes of upregulated differentially expressed genes (DEGs) in SETI_wt across the indicated treatments.

Supplemental tables can be accessed online at (https://doi.org/10.1016/j.celrep.2025.115394)

References

1. Dodds, P.N., and Rathjen, J.P. (2010). Plant immunity: towards an integrated view of plant-pathogen interactions. Nat. Rev. Genet. *11*, 539–548. 10.1038/nrg2812.

2. Duxbury, Z., Wu, C.-H., and Ding, P. (2021). A comparative overview of the intracellular guardians of plants and animals: nlrs in innate immunity and beyond. Annu. Rev. Plant Biol. *72*, 155–184. 10.1146/annurev-arplant-080620-104948.

3. Jones, J.D.G., and Dangl, J.L. (2006). The plant immune system. Nature *444*, 323–329. 10.1038/nature05286.

4. Ngou, B.P.M., Ahn, H.-K., Ding, P., and Jones, J.D.G. (2021). Mutual potentiation of plant immunity by cell-surface and intracellular receptors. Nature *592*, 110–115. 10.1038/s41586-021-03315-7.

5. Yuan, M., Ngou, B.P.M., Ding, P., and Xin, X.-F. (2021). PTI-ETI crosstalk: an integrative view of plant immunity. Curr. Opin. Plant Biol. *62*, 102030. 10.1016/j.pbi.2021.102030.

6. Parker, J.E., Hessler, G., and Cui, H. (2022). A new biochemistry connecting pathogen detection to induced defense in plants. New Phytol. *234*, 819–826. 10.1111/nph.17924.

7. Wiermer, M., Feys, B.J., and Parker, J.E. (2005). Plant immunity: the EDS1 regulatory node. Curr. Opin. Plant Biol. *8*, 383–389. 10.1016/j.pbi.2005.05.010.

8. Wagner, S., Stuttmann, J., Rietz, S., Guerois, R., Brunstein, E., Bautor, J., Niefind, K., and Parker, J.E. (2013). Structural basis for signaling by exclusive EDS1 heteromeric complexes with SAG101 or PAD4 in plant innate immunity. Cell Host Microbe *14*, 619–630. 10.1016/j.chom.2013.11.006.

9. Bhattacharjee, S., Halane, M.K., Kim, S.H., and Gassmann, W. (2011). Pathogen effectors target Arabidopsis EDS1 and alter its interactions with immune regulators. Science *334*, 1405–1408. 10.1126/science.1211592.

10. Zhu, S., Jeong, R.-D., Venugopal, S.C., Lapchyk, L., Navarre, D., Kachroo, A., and Kachroo, P. (2011). SAG101 forms a ternary complex with EDS1 and PAD4 and is required for resistance signaling against turnip crinkle virus. PLoS Pathog. *7*, e1002318. 10.1371/journal.ppat.1002318.

11. Vlot, A.C., Dempsey, D.A., and Klessig, D.F. (2009). Salicylic Acid, a multifaceted hormone to combat disease. Annu. Rev. Phytopathol. *47*, 177–206. 10.1146/annurev.phyto.050908.135202.

12. Bonardi, V., Tang, S., Stallmann, A., Roberts, M., Cherkis, K., and Dangl, J.L. (2011). Expanded functions for a family of plant intracellular immune receptors beyond specific recognition of pathogen effectors. Proc Natl Acad Sci USA *108*, 16463–16468. 10.1073/pnas.1113726108.

13. Dong, O.X., Tong, M., Bonardi, V., El Kasmi, F., Woloshen, V., Wünsch, L.K., Dangl, J.L., and Li, X. (2016). TNL-mediated immunity in Arabidopsis requires complex regulation of the

redundant ADR1 gene family. New Phytol. *210*, 960–973. 10.1111/nph.13821.

14. Castel, B., Ngou, P.-M., Cevik, V., Redkar, A., Kim, D.-S., Yang, Y., Ding, P., and Jones, J.D.G. (2019). Diverse NLR immune receptors activate defence via the RPW8-NLR NRG1. New Phytol. *222*, 966–980. 10.1111/nph.15659.

15. Wu, Z., Li, M., Dong, O.X., Xia, S., Liang, W., Bao, Y., Wasteneys, G., and Li, X. (2019). Differential regulation of TNL-mediated immune signaling by redundant helper CNLs. New Phytol. *222*, 938–953. 10.1111/nph.15665.

16. Lapin, D., Kovacova, V., Sun, X., Dongus, J.A., Bhandari, D., von Born, P., Bautor, J., Guarneri, N., Rzemieniewski, J., Stuttmann, J., et al. (2019). A Coevolved EDS1-SAG101-NRG1 Module Mediates Cell Death Signaling by TIR-Domain Immune Receptors. Plant Cell *31*, 2430–2455. 10.1105/tpc.19.00118.

17. Saile, S.C., Jacob, P., Castel, B., Jubic, L.M., Salas-Gonzáles, I., Bäcker, M., Jones, J.D.G., Dangl, J.L., and El Kasmi, F. (2020). Two unequally redundant "helper" immune receptor families mediate Arabidopsis thaliana intracellular "sensor" immune receptor functions. PLoS Biol. *18*, e3000783. 10.1371/journal.pbio.3000783.

18. Collier, S.M., Hamel, L.-P., and Moffett, P. (2011). Cell death mediated by the N-terminal domains of a unique and highly conserved class of NB-LRR protein. Mol. Plant Microbe Interact. *24*, 918–931. 10.1094/MPMI-03-11-0050.

19. Sun, X., Lapin, D., Feehan, J.M., Stolze, S.C., Kramer, K., Dongus, J.A., Rzemieniewski, J., Blanvillain-Baufumé, S., Harzen, A., Bautor, J., et al. (2021). Pathogen effector recognition-dependent association of NRG1 with EDS1 and SAG101 in TNL receptor immunity. Nat. Commun. *12*, 3335. 10.1038/s41467-021-23614-x.

20. Wu, Z., Tian, L., Liu, X., Zhang, Y., and Li, X. (2021). TIR signal promotes interactions between lipase-like proteins and ADR1-L1 receptor and ADR1-L1 oligomerization. Plant Physiol. *187*, 681–686. 10.1093/plphys/kiab305.

21. He, Z., Webster, S., and He, S.Y. (2022). Growth-defense trade-offs in plants. Curr. Biol. *32*, R634–R639. 10.1016/j.cub.2022.04.070.

22. van Wersch, R., Li, X., and Zhang, Y. (2016). Mighty dwarfs: arabidopsis autoimmune mutants and their usages in genetic dissection of plant immunity. Front. Plant Sci. *7*, 1717. 10.3389/fpls.2016.01717.

23. Denancé, N., Sánchez-Vallet, A., Goffner, D., and Molina, A. (2013). Disease resistance or growth: the role of plant hormones in balancing immune responses and fitness costs. Front. Plant Sci. *4*, 155. 10.3389/fpls.2013.00155.

24. Ngou, B.P.M., Ahn, H.-K., Ding, P., Redkar, A., Brown, H., Ma, Y., Youles, M., Tomlinson, L., and Jones, J.D.G. (2020). Estradiol-inducible AvrRps4 expression reveals distinct properties of TIR-NLR-mediated effector-triggered immunity. J. Exp. Bot. *71*, 2186–2197. 10.1093/jxb/erz571.

25. Cooper, A., and Ton, J. (2022). Immune priming in plants: from the onset to transgenerational maintenance. Essays Biochem. *66*, 635–646. 10.1042/EBC20210082.

26. Liu, J., Ding, P., Sun, T., Nitta, Y., Dong, O., Huang, X., Yang, W., Li, X., Botella, J.R., and Zhang, Y. (2013). Heterotrimeric G proteins serve as a converging point in plant defense signaling activated by multiple receptor-like kinases. Plant Physiol. *161*, 2146–2158. 10.1104/pp.112.212431.

27. Mur, L.A.J., Aubry, S., Mondhe, M., Kingston-Smith, A., Gallagher, J., Timms-Taravella, E., James, C., Papp, I., Hörtensteiner, S., Thomas, H., et al. (2010). Accumulation of chlorophyll catabolites photosensitizes the hypersensitive response elicited by Pseudomonas syringae in Arabidopsis. New Phytol. *188*, 161–174. 10.1111/j.1469-8137.2010.03377.x.

28. Mur, L.A.J., Kenton, P., Lloyd, A.J., Ougham, H., and Prats, E. (2008). The hypersensitive response; the centenary is upon us but how much do we know? J. Exp. Bot. *59*, 501–520. 10.1093/jxb/erm239.

29. Pruitt, R.N., Locci, F., Wanke, F., Zhang, L., Saile, S.C., Joe, A., Karelina, D., Hua, C., Fröhlich, K., Wan, W.-L., et al. (2021). The EDS1-PAD4-ADR1 node mediates Arabidopsis pattern-triggered immunity. Nature *598*, 495–499. 10.1038/s41586-021-03829-0.

30. Saraçli, S., Doğan, N., and Doğan, İ. (2013). Comparison of hierarchical cluster analysis methods by cophenetic correlation. J. Inequal. Appl. *2013*, 203. 10.1186/1029-242X-2013-203.

31. Ding, P., Rekhter, D., Ding, Y., Feussner, K., Busta, L., Haroth, S., Xu, S., Li, X., Jetter, R., Feussner, I., et al. (2016). Characterization of a pipecolic acid biosynthesis pathway required for systemic acquired resistance. Plant Cell *28*, 2603–2615. 10.1105/tpc.16.00486.

32. Ding, P., and Ding, Y. (2020). Stories of salicylic acid: A plant defense hormone. Trends Plant Sci. *25*, 549–565. 10.1016/j.tplants.2020.01.004.

33. Rojas, C.M., Senthil-Kumar, M., Tzin, V., and Mysore, K.S. (2014). Regulation of primary plant metabolism during plant-pathogen interactions and its contribution to plant defense. Front. Plant Sci. *5*, 17. 10.3389/fpls.2014.00017.

34. Du, Y., and Scheres, B. (2018). Lateral root formation and the multiple roles of auxin. J. Exp. Bot. *69*, 155–167. 10.1093/jxb/erx223.

35. Rietz, S., Stamm, A., Malonek, S., Wagner, S., Becker, D., Medina-Escobar, N., Corina Vlot, A., Feys, B.J., Niefind, K., and Parker, J.E. (2011). Different roles of Enhanced Disease Susceptibility1 (EDS1) bound to and dissociated from Phytoalexin Deficient4 (PAD4) in Arabidopsis immunity. New Phytol. *191*, 107–119. 10.1111/j.1469-8137.2011.03675.x.

36. Gantner, J., Ordon, J., Kretschmer, C., Guerois, R., and Stuttmann, J. (2019). An EDS1-SAG101 Complex Is Essential for TNL-Mediated Immunity in Nicotiana benthamiana. Plant Cell *31*, 2456–2474. 10.1105/tpc.19.00099.

37. Qi, T., Seong, K., Thomazella, D.P.T., Kim, J.R., Pham, J., Seo, E., Cho, M.-J., Schultink, A., and Staskawicz, B.J. (2018). NRG1 functions downstream of EDS1 to regulate TIR-NLR-mediated plant immunity in Nicotiana benthamiana. Proc Natl Acad Sci USA *115*, E10979–E10987. 10.1073/pnas.1814856115.

38. Feehan, J.M., Wang, J., Sun, X., Choi, J., Ahn, H.-K., Ngou, B.P.M., Parker, J.E., and Jones, J.D.G. (2023). Oligomerization of a plant helper NLR requires cell-surface and intracellular immune receptor activation. Proc Natl Acad Sci USA *120*, e2210406120. 10.1073/pnas.2210406120.

39. de Ronde, D., Butterbach, P., and Kormelink, R. (2014). Dominant resistance against plant viruses. Front. Plant Sci. *5*, 307. 10.3389/fpls.2014.00307.

40. Feys, B.J., Wiermer, M., Bhat, R.A., Moisan, L.J., Medina-Escobar, N., Neu, C., Cabral, A., and Parker, J.E. (2005). Arabidopsis SENESCENCE-ASSOCIATED GENE101 stabilizes and signals within an ENHANCED DISEASE SUSCEPTIBILITY1 complex in plant innate immunity. Plant Cell *17*, 2601–2613. 10.1105/tpc.105.033910.

41. Bonardi, V., Cherkis, K., Nishimura, M.T., and Dangl, J.L. (2012). A new eye on NLR proteins: focused on clarity or diffused by complexity? Curr. Opin. Immunol. *24*, 41–50. 10.1016/j.coi.2011.12.006.

42. Bjornson, M., Pimprikar, P., Nürnberger, T., and Zipfel, C. (2021). The transcriptional landscape of Arabidopsis thaliana pattern-

triggered immunity. Nat. Plants *7*, 579–586. 10.1038/s41477-021-00874-5.

43. Ding, P., Sakai, T., Krishna Shrestha, R., Manosalva Perez, N., Guo, W., Ngou, B.P.M., He, S., Liu, C., Feng, X., Zhang, R., et al. (2021). Chromatin accessibility landscapes activated by cell-surface and intracellular immune receptors. J. Exp. Bot. *72*, 7927–7941. 10.1093/jxb/erab373.

44. Locci, F., Wang, J., and Parker, J.E. (2023). TIR-domain enzymatic activities at the heart of plant immunity. Curr. Opin. Plant Biol. *74*, 102373. 10.1016/j.pbi.2023.102373.

45. Peart, J.R., Mestre, P., Lu, R., Malcuit, I., and Baulcombe, D.C. (2005). NRG1, a CC-NB-LRR protein, together with N, a TIR-NB-LRR protein, mediates resistance against tobacco mosaic virus. Curr. Biol. *15*, 968–973. 10.1016/j.cub.2005.04.053.

46. Thomas, W.J., Thireault, C.A., Kimbrel, J.A., and Chang, J.H. (2009). Recombineering and stable integration of the Pseudomonas syringae pv. syringae 61 hrp/hrc cluster into the genome of the soil bacterium Pseudomonas fluorescens Pf0-1. Plant J. *60*, 919–928. 10.1111/j.1365-313X.2009.03998.x.

47. Bjornson, M., Kajala, K., Zipfel, C., and Ding, P. (2020). Low-cost and High-throughput RNA-seq Library Preparation for Illumina Sequencing from Plant Tissue. Bio Protoc *10*, e3799. 10.21769/BioProtoc.3799.

48. Andrews, S. (2023). FastQC.

49. Zhang, R., Kuo, R., Coulter, M., Calixto, C.P.G., Entizne, J.C., Guo, W., Marquez, Y., Milne, L., Riegler, S., Matsui, A., et al. (2022). A high-resolution single-molecule sequencing-based Arabidopsis transcriptome using novel methods of Iso-seq analysis. Genome Biol. *23*, 149. 10.1186/s13059-022-02711-0.

50. Bray, N.L., Pimentel, H., Melsted, P., and Pachter, L. (2016). Near-optimal probabilistic RNA-seq quantification. Nat. Biotechnol. *34*, 525–527. 10.1038/nbt.3519.

51. Guo, W., Tzioutziou, N.A., Stephen, G., Milne, I., Calixto, C.P., Waugh, R., Brown, J.W.S., and Zhang, R. (2021). 3D RNA-seq: a powerful and flexible tool for rapid and accurate differential expression and alternative splicing analysis of RNA-seq data for biologists. RNA Biol. *18*, 1574–1587. 10.1080/15476286.2020.1858253.

52. Risso, D., Ngai, J., Speed, T.P., and Dudoit, S. (2014). Normalization of RNA-seq data using factor analysis of control genes or samples. Nat. Biotechnol. *32*, 896–902. 10.1038/nbt.2931.

53. Robinson, M.D., and Oshlack, A. (2010). A scaling normalization method for differential expression analysis of RNA-seq data. Genome Biol. *11*, R25. 10.1186/gb-2010-11-3-r25.

54. Law, C.W., Chen, Y., Shi, W., and Smyth, G.K. (2014). voom: Precision weights unlock linear model analysis tools for RNA-seq read counts. Genome Biol. *15*, R29. 10.1186/gb-2014-15-2-r29.

55. Ritchie, M.E., Phipson, B., Wu, D., Hu, Y., Law, C.W., Shi, W., and Smyth, G.K. (2015). limma powers differential expression analyses for RNA-sequencing and microarray studies. Nucleic Acids Res. *43*, e47. 10.1093/nar/gkv007.

56. Kolberg, L., Raudvere, U., Kuzmin, I., Adler, P., Vilo, J., and Peterson, H. (2023). g:Profiler-interoperable web service for functional enrichment analysis and gene identifier mapping (2023 update). Nucleic Acids Res. *51*, W207–W212. 10.1093/nar/gkad347.

57. Sohn, K.H., Zhang, Y., and Jones, J.D.G. (2009). The Pseudomonas syringae effector protein, AvrRPS4, requires in planta processing and the KRVY domain to function. Plant J. *57*, 1079–1091. 10.1111/j.1365-313X.2008.03751.x.

58. Petnicki-Ocwieja, T., van Dijk, K., and Alfano, J.R. (2005). The hrpK operon of Pseudomonas syringae pv. tomato DC3000 encodes two proteins secreted by the type III (Hrp) protein secretion system: HopB1 and HrpK, a putative type III translocator. J. Bacteriol. *187*, 649–663. 10.1128/JB.187.2.649-663.2005.

59. Chazaux, M., Schiphorst, C., Lazzari, G., and Caffarri, S. (2022). Precise estimation of chlorophyll a, b and carotenoid content by deconvolution of the absorption spectrum and new simultaneous equations for Chl determination. Plant J. *109*, 1630–1648. 10.1111/tpj.15643.

60. Gu, Z. (2022). Complex heatmap visualization. iMeta *1*, e43. 10.1002/imt2.43.

61. Lex, A., Gehlenborg, N., Strobelt, H., Vuillemot, R., and Pfister, H. (2014). Upset: visualization of intersecting sets. IEEE Trans. Vis. Comput. Graph. *20*, 1983–1992. 10.1109/TVCG.2014.2346248.

62. Blighe, K., Rana, S., and Lewis, M. (2018). EnhancedVolcano: Publication-ready volcano plots with enhanced colouring and labeling. Bioconductor. 10.18129/b9.bioc.enhancedvolcano.

63. Iannone, R., Cheng, J., Schloerke, B., Hughes, E., Lauer, A., Seo, J., Brevoort, K., and Roy, O. (2024). gt: Easily Create Presentation-Ready Display Tables.

64. Mock, T. (2023). gtExtras: Extending “gt” for Beautiful HTML Tables.

65. Wickham, H., Averick, M., Bryan, J., Chang, W., McGowan, L., François, R., Grolemund, G., Hayes, A., Henry, L., Hester, J., et al. (2019). Welcome to the tidyverse. JOSS *4*, 1686. 10.21105/joss.01686.

66. Graves, S., Piepho, H.-P., and Luciano Selzer with help from Sundar Dorai-Raj (2023). multcompView: Visualizations of Paired Comparisons.

67. de Mendiburu, F. (2023). agricolae: Statistical Procedures for Agricultural Research.

68. Kassambara, A. (2023). ggpubr: “ggplot2” Based Publication Ready Plots.

69. Wickham, H. (2023). stringr: Simple, Consistent Wrappers for Common String Operations.

70. Gherardi, V. (2021). r2r: R-Object to R-Object Hash Maps.

71. Gu, Z., Gu, L., Eils, R., Schlesner, M., and Brors, B. (2014). circlize Implements and enhances circular visualization in R. Bioinformatics *30*, 2811–2812. 10.1093/bioinformatics/btu393.